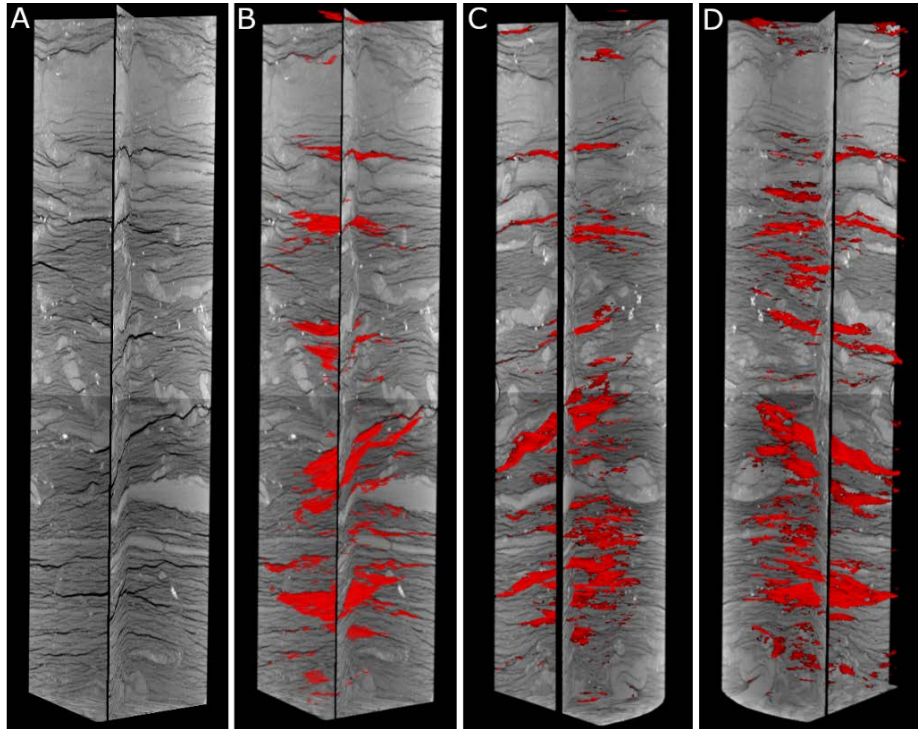




NATIONAL ENERGY TECHNOLOGY LABORATORY



Computed Tomography Scanning and Geophysical Measurements of the Rogersville Shale from the Smith #1 Well

4 September 2018



U.S. DEPARTMENT OF
ENERGY



NATIONAL
ENERGY
TECHNOLOGY
LABORATORY

Office of Fossil Energy

NETL-TRS-16-2018

Disclaimer

This report was prepared as an account of work sponsored by an agency of the United States Government. Neither the United States Government nor any agency thereof, nor any of their employees, makes any warranty, express or implied, or assumes any legal liability or responsibility for the accuracy, completeness, or usefulness of any information, apparatus, product, or process disclosed, or represents that its use would not infringe privately owned rights. Reference therein to any specific commercial product, process, or service by trade name, trademark, manufacturer, or otherwise does not necessarily constitute or imply its endorsement, recommendation, or favoring by the United States Government or any agency thereof. The views and opinions of authors expressed therein do not necessarily state or reflect those of the United States Government or any agency thereof.

Cover Illustration: Visualization of open fractures in the Smith #1 core at depth 11,147.5 to 11,147.9 ft. The images represent: A) orthographic planes through the CT volume, B-D) 3D volume of fractures in orthographic planes shown at respective 0°, 120°, and 240° rotations.

Suggested Citation: Mackey, P.; Paronish, T.; Brown, S.; Moore, J.; Crandall, D.; Dinterman, P.; Moore, J. *Computed Tomography Scanning and Geophysical Measurements of the Rogersville Shale from the Smith #1 Well*; NETL-TRS-16-2018; NETL Technical Report Series; U.S. Department of Energy, National Energy Technology Laboratory: Morgantown, WV, 2018; p 48. DOI: 10.18141/1468399.

An electronic version of this report can be found at:

<http://netl.doe.gov/research/on-site-research/publications/featured-technical-reports>
<https://edx.netl.doe.gov/ucr>

The data in this report can be accessed from NETL's Energy Data eXchange ([EDX](#)) online system (<https://edx.netl.doe.gov>) using the following link:
<https://edx.netl.doe.gov/dataset/roger-well>

Computed Tomography Scanning and Geophysical Measurements of the Rogersville Shale from the Smith #1 Well

**Paige Mackey^{1,2}, Thomas Paronish^{1,2}, Sarah Brown^{1,3}, Johnathan Moore^{1,3},
Dustin Crandall¹, Phil Dinterman⁴, Jessica Moore⁴**

**¹U.S. Department of Energy, National Energy Technology Laboratory,
3610 Collins Ferry Road, Morgantown, WV 26507**

**²U.S. Department of Energy, National Energy Technology Laboratory, ORISE,
3610 Collins Ferry Road, Morgantown, WV 26507**

**³U.S. Department of Energy, National Energy Technology Laboratory, AECOM,
3610 Collins Ferry Road, Morgantown, WV 26507**

**⁴West Virginia Geological and Economic Survey, 1 Mont Chateau Road, Morgantown, WV
26508**

NETL-TRS-16-2018

4 September 2018

NETL Contacts:

Dustin Crandall, Principal Investigator

Alexandra Hakala, Technical Portfolio Lead

Bryan Morreale, Executive Director, Research & Innovation Center

This page intentionally left blank.

Table of Contents

ABSTRACT	1
1. INTRODUCTION	2
2. CORE DESCRIPTION	6
2.1 CORE PHOTOGRAPHS.....	7
3. DATA ACQUISITION AND METHODOLOGY	13
3.1 CORE LOGGING.....	13
3.2 INDUSTRIAL CT SCANNING.....	16
3.3 MEDICAL CT SCANNING.....	17
3.4 DATA COMPILATION.....	17
4. RESULTS	18
4.1 MEDICAL CT SCANS	18
4.2 SMITH #1	19
4.3 INDUSTRIAL CT SCANS.....	24
4.4 ADDITIONAL CT DATA	27
4.5 DUAL ENERGY CT SCANNING	27
4.6 COMPILED CORE LOG	29
5. DISCUSSION	35
6. REFERENCES	37

This page intentionally left blank.

List of Figures

Figure 1: Smith #1 well location map on top of Goggle Earth imagery..... 3

Figure 2: Smith #1 well location map including Rogersville Shale structure contours (feet below mean sea level) from Hickman et al. (2015). Structure contours intervals are 500 ft, modified from Hickman et al. (2015). 4

Figure 3: Smith #1 well location map including isopach contours of the Rogersville Shale. Contours intervals are 1,000 ft, modified from Hickman et al. (2015)..... 5

Figure 4: Smith #1 core photographs, from 11,135 to 11,145 ft. 7

Figure 5: Smith #1 core photographs, from 11,146 to 11,157.3 ft. 8

Figure 6: Smith #1 core photographs, from 11,157.3 to 11,168 ft. 9

Figure 7: Smith #1 core photographs, from 11,168 to 11,179.5 ft. 10

Figure 8: Smith #1 core photographs, from 11,179.5 to 11,190 ft. 11

Figure 9: Smith #1 core photographs, from 11,191 to 11,200.5 ft. 12

Figure 10: Representation of generalized MSCL with all attached instruments. From Geotek Ltd., Geotek Multi-Sensor Core Logger Flyer, Daventry, UK (2009). 13

Figure 11: Periodic table showing elements measurable by the Innov-X® X-Ray Fluorescence Spectrometer. 15

Figure 12: North Star Imaging Inc. M-5000® Industrial Computed Tomography Scanner at NETL used for core analysis..... 16

Figure 13: Medical CT at the NETL used for core analysis. 17

Figure 14: 2D isolated planes through the vertical center of the medical CT scans of the Smith #1 core from 11,135 to 11,148 ft. 19

Figure 15: 2D isolated planes through the vertical center of the medical CT scans of the Smith #1 core from 11,149 to 11,162 ft. 20

Figure 16: 2D isolated planes through the vertical center of the medical CT scans of the Smith #1 core from 11,162 to 11,177 ft. 21

Figure 17: 2D isolated planes through the vertical center of the medical CT scans of the Smith #1 core from 11,177 to 11,190 ft. 22

Figure 18: 2D isolated planes through the vertical center of the medical CT scans of the Smith #1 core from 11,191 to 11,200.5 ft. 23

Figure 19: Visualization of features from the Smith #1 core at depth 11,147.5–11,147.9 ft. The images represent: A) Core photograph with scale in cm, B) 3D volumetric CT scan, C) Orthographic planes through the CT volume..... 24

Figure 20: Visualization of features from the Smith #1 core at depth 11,147.7–11,147.9 ft. The images represent: A) orthographic planes through the CT volume, B) 3D volume of sand and silt in orthographic planes showing soft sediment deformation and filled burrows, and C) complete 3D volume with features distinguished by the colors from the legend. 25

Figure 21: Representation of open fractures in the Smith #1 core at depth 11,147.5–11,147.9 ft. The images display: A) orthographic planes through the CT volume, B–C) 3D volume of fractures in orthographic planes shown at respective 0°, 120°, and 240° rotations..... 26

Figure 22: Single image from a video file available on EDX showing variation of the Smith #1 core from 11,160 to 11,162 ft. The image above shows the variation in composition within the matrix perpendicular to the core length. Note the bright (high density) nodule in the cross plane of the image..... 27

List of Figures (cont.)

Figure 23: Photon interactions at varying energies: a) photoelectric absorption, b) Compton scattering. Modified from NDT Resource Center (2018).....	28
Figure 24: Compiled core log for Smith #1 well, from 11,135 to 11,168 ft.....	31
Figure 25: Compiled core log for Smith #1 well, from 11,168 to 11,200 ft.....	32
Figure 26: Compiled core log with elemental ratios for Smith #1 well, from 11,135 to 11,168 ft.	33
Figure 27: Compiled core log with elemental ratios for Smith #1 well, from 11,168 to 11,200 ft.	34

List of Tables

Table 1: Magnetic susceptibility values for common minerals (Modified from Geotek Ltd. Multi-Sensor Core Logger Manual, Version 05-10, 2010).....	14
Table 2: Dual energy calibration standards	28
Table 3: Dual energy calibration standards	28

Acronyms, Abbreviations, and Symbols

Term	Description
2D	Two-dimensional
3D	Three-dimensional
CT	Computed tomography
CTN	Computed tomography number
EDX	NETL's Energy Data eXchange
HU	Hounsfield units
MSCL	Multi-Sensor Core Logger
NETL	National Energy Technology Laboratory
WVGES	West Virginia Geological and Economic Survey
XRF	X-ray fluorescence

This page intentionally left blank.

Acknowledgments

This work was completed at the National Energy Technology Laboratory (NETL) with support from U.S. Department of Energy's (DOE) Office of Fossil Energy Oil & Gas Program. The authors wish to acknowledge Bryan Morreale and Alexandra Hakala (NETL Research & Innovation Center), Jared Ciferno (NETL Technology Development and Integration Center), and Elena Melchert (DOE Office of Fossil Energy) for programmatic guidance, direction, and support.

The authors would like to thank Scott Workman, Bryan Tennant, and Karl Jarvis for data collection and technical support. Thank you to West Virginia Geological and Economic Survey (WVGES) for allowing us to work with this core. Thank you to Kelly Rose, Dustin McIntyre, and Mark McKoy for laboratory support. This research was supported in part by appointments from the NETL Research Participation Program, sponsored by the U.S. DOE and administered by the Oak Ridge Institute for Science and Education.

This page intentionally left blank.

ABSTRACT

The computed tomography (CT) facilities and the Multi-Sensor Core Logger (MSCL) at the National Energy Technology Laboratory (NETL) Morgantown, West Virginia site were used to characterize a core from the Rogersville Shale. This sample was taken from a vertical well, the Jay P. Smith #1 well (47-099-1572), drilled in Wayne County, West Virginia by the Exxon Company in the Elmwood Prospect. The core is comprised primarily of the Rogersville Shale from depths of 11,135 to 11,200.5 ft. This unit is a potential Cambrian oil/gas target, making it of recent interest to multiple groups. The core was provided by the West Virginia Geologic and Economic Survey (WVGES).

The primary impetus of this work is a collaboration between WVGES and NETL to characterize core from multiple wells to better understand the structure and variation of key formations in West Virginia (e.g., Crandall et al., 2018a,b). As part of this effort, bulk scans of core were obtained from the Smith #1 well. This report, and the associated scans, provide detailed datasets not typically available from unconventional shales for analysis. The resultant datasets are presented in this report, and can be accessed from NETL's Energy Data eXchange (EDX) online system using the following link: <https://edx.netl.doe.gov/dataset/roger-well>.

All equipment and techniques used were non-destructive, enabling future examinations to be performed on these cores. None of the equipment used was suitable for direct visualization of the shale pore space, although fractures and discontinuities were detectable with the methods tested. Low resolution CT imagery with the NETL medical CT scanner was performed on the entire core. Qualitative analysis of the medical CT images, coupled with X-ray fluorescence (XRF), P-wave, and magnetic susceptibility measurements from the MSCL were useful in identifying zones of interest for more detailed analysis as well as fractured zones. The ability to quickly identify key areas for more detailed study with higher resolution will save time and resources in future studies. The combination of methods used provided a multi-scale analysis of this core and provides both a macro and micro description of the core that is relevant for many subsurface energy-related examinations that have traditionally been performed at NETL.

1. INTRODUCTION

Evaluation of reservoir samples can support resource estimation and determination of effective extraction methodologies. While it is common for commercial entities to perform these characterizations, the resources necessary to conduct these analyses are not always available to the broader interest base, such as state agencies or research-based consortiums. To meet the growing need for comprehensive, high-quality lithologic data for collaborative research initiatives, the National Energy Technology Laboratory (NETL) has used its available resources to analyze core with both existing techniques and new, innovative methodologies. The combination of new and old techniques allowed the NETL to develop a systematic approach for the evaluation of cores. In this report, data collected from a Rogersville Shale well in Wayne County, West Virginia are presented as one part of a broader collaborative effort by West Virginia Geologic and Economic Survey (WVGES) and NETL to better characterize important, spatially heterogeneous, formations in West Virginia.

In this study, the primary objective was to characterize core from depth with methods not available to most researchers. The data is presented in several formats here and online that are potentially useful for various analyses. Detailed analysis is not presented in this report as the research objective was not to do a site characterization, but rather to develop the data for others to utilize and to create a digital representation of the core that could be preserved.

The core described here is from the Exxon Smith #1 well (99-1572), which was drilled through the Rogersville Shale, a potential Cambrian oil/gas target that has had recent interest due to some high reported values of total organic carbon (1.20 to 4.40%) (Ryder et al., 2014; Harris et al., 2004). The Middle Cambrian Rogersville Shale is within the Conasauga Group and is known to be an organic-rich dark shale mixed with siltstone and carbonates. The geographic coordinates for the well are UTM E 365683.3, UTM N 4231537.9 (UTM NAD83), with an API No: 4709901572 (Figures 1, 2, 3). The well pad elevation was 594 ft. As shown in Figures 2 and 3, the Rogersville Shale in this area is expected between a depth of 9,500–10,000 ft below sea level, though this core is deeper, and to be of approximately 700 to 800 ft thick. The section of particular interest due to source rock potential and favorable oil-source rock correlations (Ryder et al., 2014) is 123 ft thick Cambrian marine dark gray shale with thin sandstone beds, minor calcite cement, bioturbation, cross lamination and fossils (mainly brachiopods).

The Rogersville Shale thickness varies depending on location with deposition limited to within the Rome Trough, an Early to Middle Cambrian extensional graben which was part of the interior rift system that formed during the opening of the Iapetus Ocean. The Rome Trough extends from northern Tennessee to southwestern New York. Deposition of the Rogersville Shale occurred during active extension of the Rome Trough.

As part of this collaboration between WVGES and NETL to characterize core from multiple wells to better understand the structure and variation of key formations, bulk scans of core were obtained which provided base-line information on sample condition and characteristics using fast scanning techniques on large batches of samples.

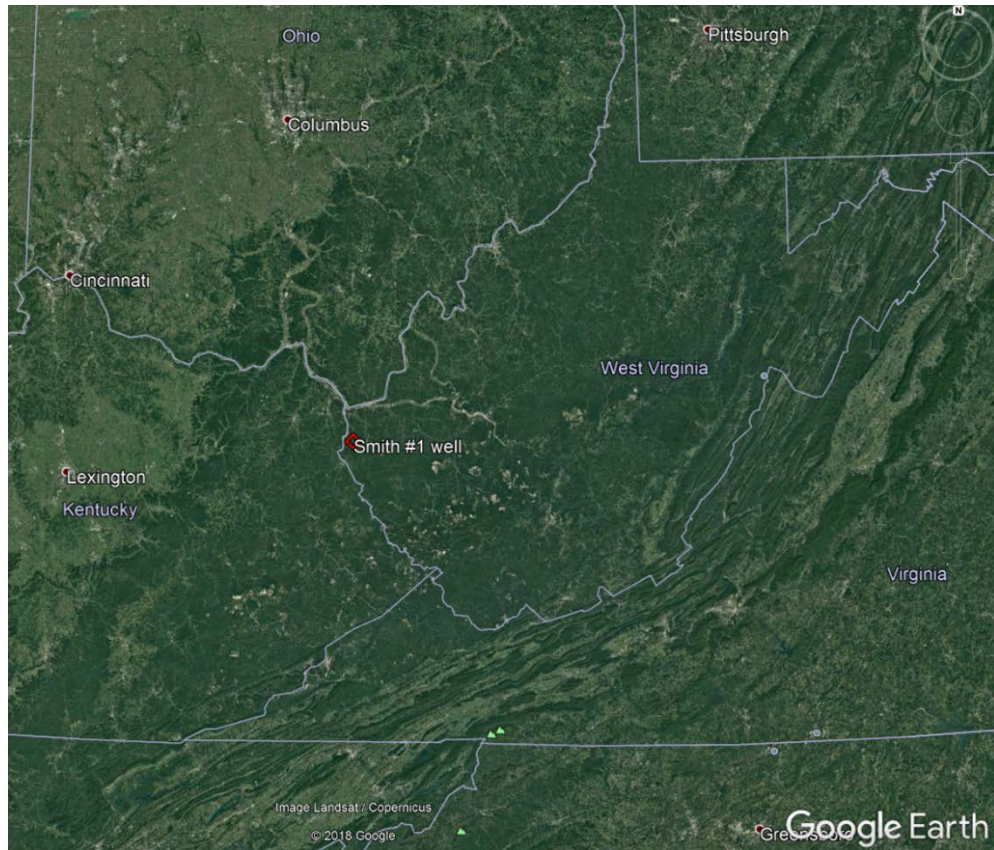


Figure 1: Smith #1 well location map on top of Goggle Earth imagery.

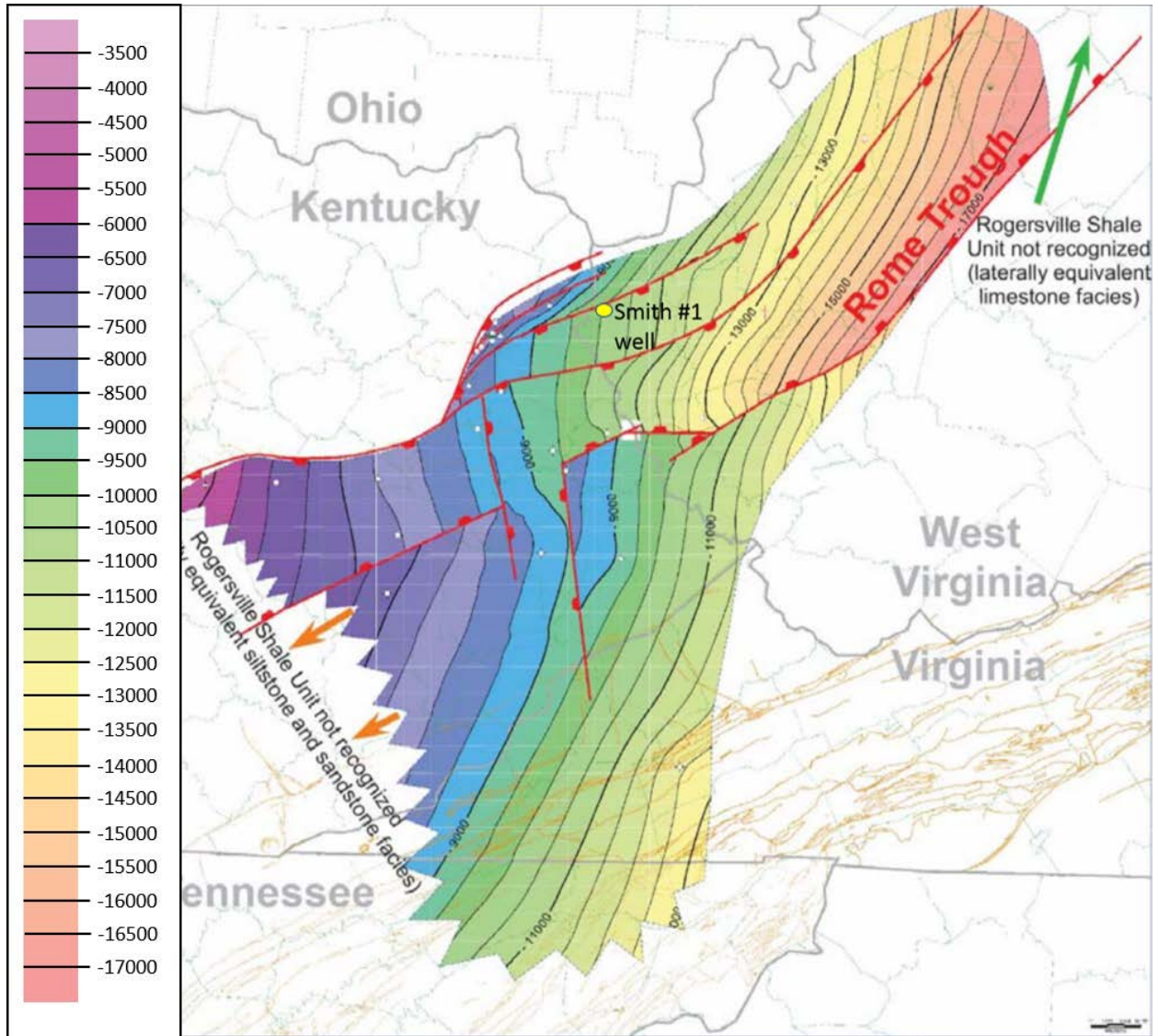


Figure 2: Smith #1 well location map including Rogersville Shale structure contours (feet below mean sea level) from Hickman et al. (2015). Structure contours intervals are 500 ft, modified from Hickman et al. (2015).

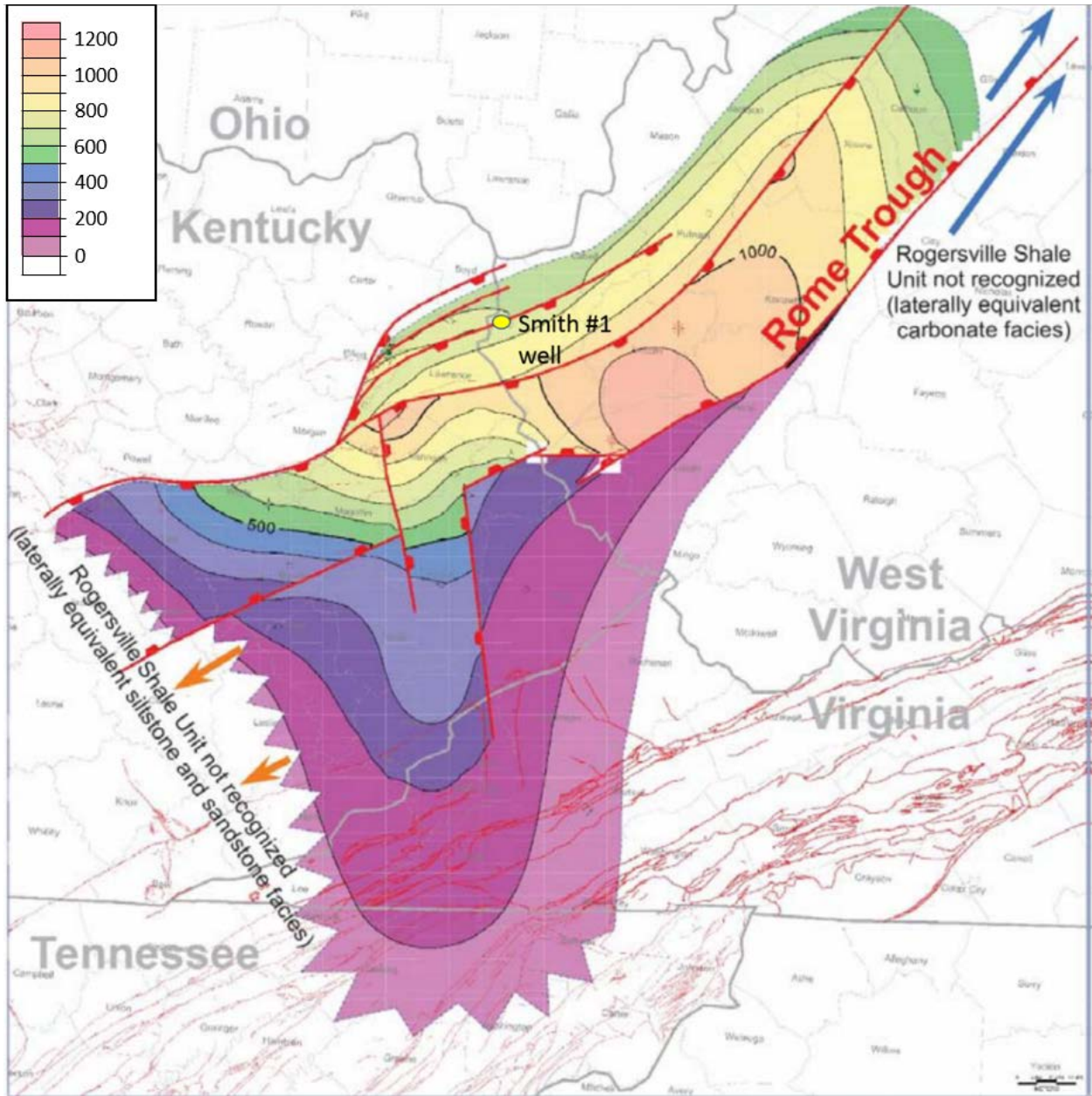


Figure 3: Smith #1 well location map including isopach contours of the Rogersville Shale. Contours intervals are 1,000 ft, modified from Hickman et al. (2015).

2. CORE DESCRIPTION

The Rogersville Shale in the Smith #1 well contains a fine-grained, dark gray shale with thin laminae of very fine-grained sandstone and/or siltstone. Parts are fossiliferous (mainly brachiopods), with sandstone and siltstone filled burrows prevalent throughout. Layer parallel fractures are common and are frequently spaced ~0.1 cm apart. Some of the sand and siltstone laminae are cross bedded. Rounded clasts of lighter, sandstone material are numerous; some are folded and show evidence of soft sediment deformation and bioturbation. The core is triangular in shape, a result of cutting a 2/3 core in half.

2.1 CORE PHOTOGRAPHS

Photographs of the slabbed core, as received at NETL.



Figure 4: Smith #1 core photographs, from 11,135 to 11,145 ft.



Figure 5: Smith #1 core photographs, from 11,146 to 11,157.3 ft.



Figure 6: Smith #1 core photographs, from 11,157.3 to 11,168 ft.



Figure 7: Smith #1 core photographs, from 11,168 to 11,179.5 ft.

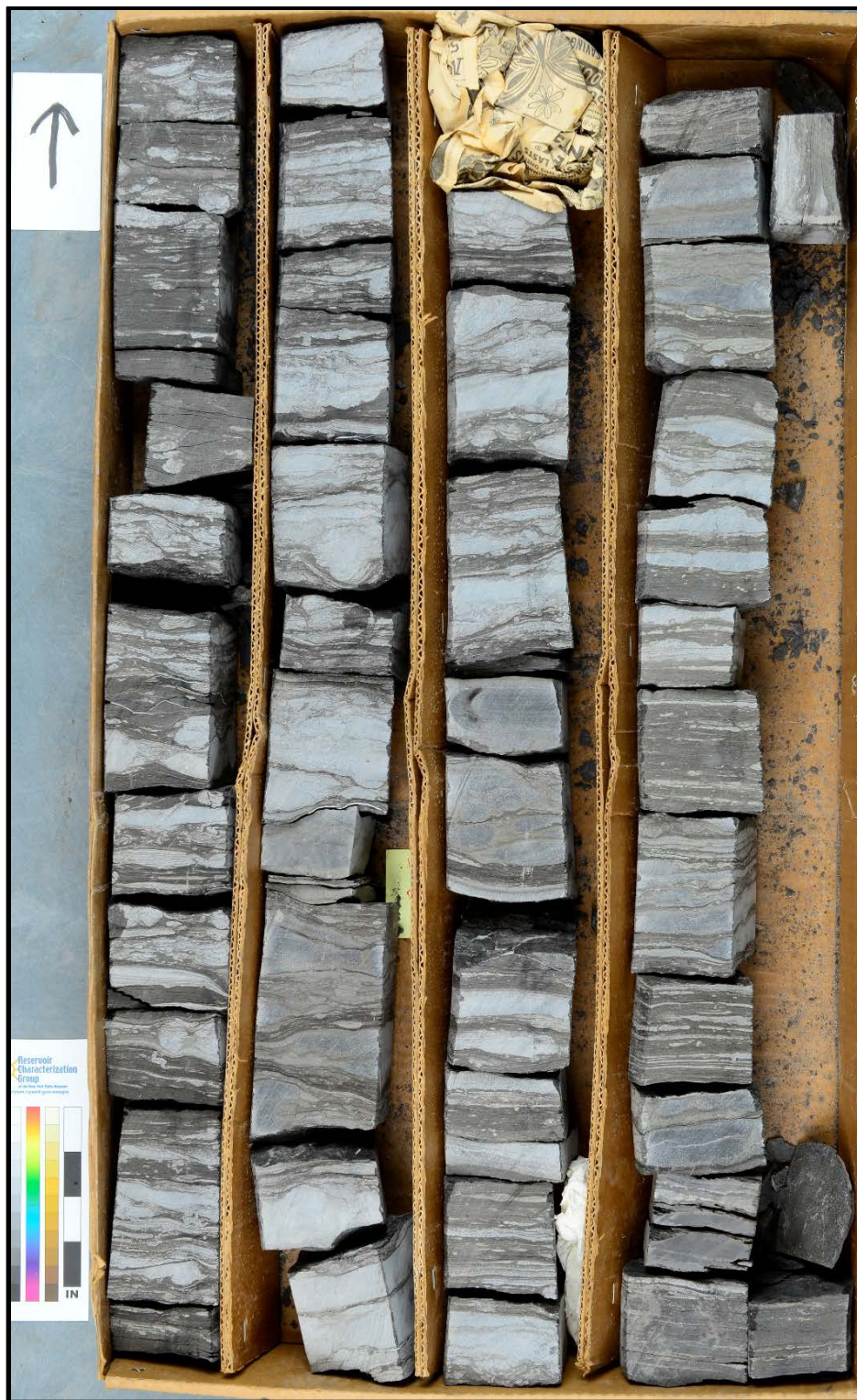


Figure 8: Smith #1 core photographs, from 11,179.5 to 11,190 ft.



Figure 9: Smith #1 core photographs, from 11,191 to 11,200.5 ft.

3. DATA ACQUISITION AND METHODOLOGY

The core was evaluated using computed tomography (CT) scanning and traditional core logging. CT scans and core logging were performed on the slabbed cores.

3.1 CORE LOGGING

Geophysical measurements of core thickness deviation, P-wave travel time, magnetic susceptibility, and attenuated gamma counts were obtained with a Geotek® Multi-Sensor Core Logging (MSCL, Figure 10) system on competent sections of core. For the slabbed core that was scanned as part of this analysis, the P-wave velocity and magnetic susceptibility were measured and reported. Additionally, the system was used to measure bulk elemental chemistry with a built-in, portable X-ray fluorescence (XRF) spectrometer. For a full description of the MSCL capabilities at NETL, please see Crandall et al. (2017).

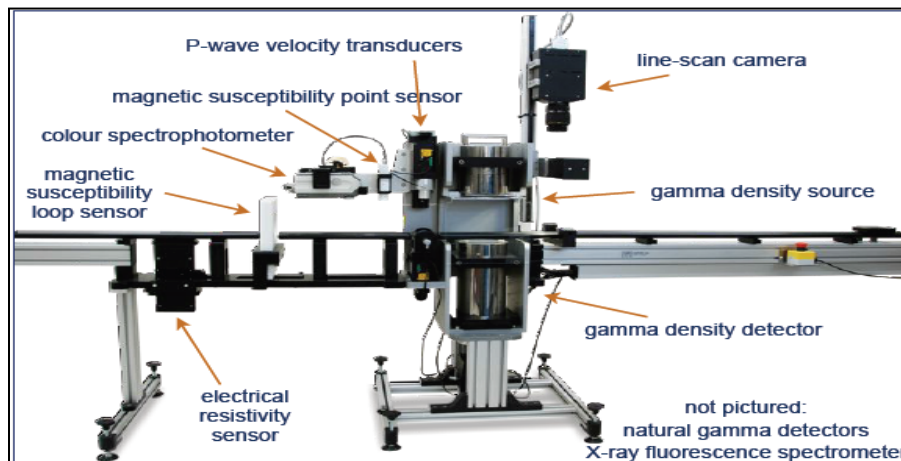


Figure 10: Representation of generalized MSCL with all attached instruments. From Geotek Ltd., Geotek Multi-Sensor Core Logger Flyer, Daventry, UK (2009).

3.1.1 Magnetic Susceptibility

Magnetic susceptibility is a measure of the degree of magnetization in the sample. The sample is passed through a ring apparatus with an oscillating magnetic field, where the interference to this field is proportional to the magnetism of the sample, and thus a relative measurement can be taken. The measurement unit used is dimensionless (described as SI units) and is based on the original calibration, which is done via stable iron oxides, and reference minerals which have known ranges of susceptibility (Table 1) (Geotek Ltd. Multi-Sensor Core Logger Manual, Version 05-10).

Table 1: Magnetic susceptibility values for common minerals (Modified from Geotek Ltd. Multi-Sensor Core Logger Manual, Version 05-10, 2010)

Mineral	χ (*10 ⁻⁶) SI
Water	9
Calcite	-7.5 to -39
Halite, Gypsum	-10 to -60
Illite, Montmorillonite	330 to 410
Pyrite	5 to 3,500
Hematite	500 to 40,000
Magnetite	1,000,000 to 5,700,000

3.1.2 P-wave Velocity

P-wave velocity measurements are performed to measure the acoustic impedance of a geologic sample with compressional waves. Acoustic impedance is a measure of how well a material transmits vibrations, which is directly proportional to density and/or material consolidation. An example of a material that has a high acoustic impedance would be air, with a wave speed of 330 m/s, whereas granite would have low acoustic impedance, with a wave speed of >5,000 m/s. These measurements can be proxies for seismic reflection coefficients and can be translated to field use when doing seismic surveys.

The software associated with the MSCL measures the travel time of the pulse with a resolution of 50 ns. The absolute accuracy of the instrument measurements is + 3 m/s with a resolution of 1.5 m/s (Geotek Ltd. Multi-Sensor Core Logger Manual, Version 05-10; Geotek Ltd., 2010).

3.1.3 X-ray Fluorescence Spectrometry

In addition to the geophysical measurements, a portable handheld Innov-X® X-Ray Fluorescence Spectrometer was used to measure relative elemental abundances of aggregated “light elements” up to and including sodium, and also various heavy elements which were measured individually (Figure 11). Elemental abundances are reported relative to the total elemental composition, i.e. out of 100% weight.

The periodic table is color-coded into two groups: Light Elements (green) and Heavy Elements (red). The Light Elements group includes Hydrogen (H), Helium (He), Lithium (Li), Beryllium (Be), Boron (B), Carbon (C), Nitrogen (N), Oxygen (O), Fluorine (F), Neon (Ne), Sodium (Na), Magnesium (Mg), Aluminum (Al), Silicon (Si), Phosphorus (P), Sulfur (S), Chlorine (Cl), and Argon (Ar). The Heavy Elements group includes Potassium (K), Calcium (Ca), Scandium (Sc), Titanium (Ti), Vanadium (V), Chromium (Cr), Manganese (Mn), Iron (Fe), Cobalt (Co), Nickel (Ni), Copper (Cu), Zinc (Zn), Gallium (Ga), Germanium (Ge), Arsenic (As), Selenium (Se), Bromine (Br), Krypton (Kr), Rubidium (Rb), Strontium (Sr), Yttrium (Y), Zirconium (Zr), Niobium (Nb), Molybdenum (Mo), Technetium (Tc), Ruthenium (Ru), Rhodium (Rh), Palladium (Pd), Silver (Ag), Cadmium (Cd), Indium (In), Tin (Sn), Antimony (Sb), Tellurium (Te), Iodine (I), Xenon (Xe), Cesium (Cs), Barium (Ba), Lanthanum (La), Cerium (Ce), Praseodymium (Pr), Neodymium (Nd), Promethium (Pm), Samarium (Sm), Europium (Eu), Gadolinium (Gd), Terbium (Tb), Dysprosium (Dy), Holmium (Ho), Erbium (Er), Thulium (Tm), Ytterbium (Yb), and Lutetium (Lu). The actinide series (Ac, Th, Pa, U, Np, Pu, Am, Cm, Bk, Cf, Es, Fm, Md, No, Lr) is shown at the bottom, with atomic numbers 89-102 and 103-118.

1 H 1.0079																	2 He 4.0026	
3 Li 6.941	4 Be 9.0122											5 B 10.811	6 C 12.011	7 N 14.007	8 O 15.999	9 F 18.998	10 Ne 20.180	
11 Na 22.990	12 Mg 24.305											13 Al 26.982	14 Si 28.086	15 P 30.974	16 S 32.065	17 Cl 35.453	18 Ar 39.948	
19 K 39.098	20 Ca 40.078	21 Sc 44.956	22 Ti 47.867	23 V 50.942	24 Cr 51.996	25 Mn 54.938	26 Fe 55.845	27 Co 58.933	28 Ni 58.693	29 Cu 63.546	30 Zn 65.39	31 Ga 69.723	32 Ge 72.61	33 As 74.922	34 Se 78.96	35 Br 79.904	36 Kr 83.80	
37 Rb 85.468	38 Sr 87.62	39 Y 88.906	40 Zr 91.224	41 Nb 92.906	42 Mo 95.94	43 Tc [98]	44 Ru 101.07	45 Rh 102.91	46 Pd 106.42	47 Ag 107.87	48 Cd 112.41	49 In 114.82	50 Sn 118.71	51 Sb 121.76	52 Te 127.60	53 I 126.90	54 Xe 131.29	
55 Cs 132.91	56 Ba 137.33	57-70 *	71 Lu 174.97	72 Hf 178.49	73 Ta 180.95	74 W 183.84	75 Re 186.21	76 Os 190.23	77 Ir 192.22	78 Pt 195.08	79 Au 196.97	80 Hg 200.59	81 Tl 204.38	82 Pb 207.2	83 Bi 208.98	84 Po [209]	85 At [210]	86 Rn [222]
87 Fr [223]	88 Ra [226]	89-102 **	103 Lr [262]	104 Rf [261]	105 Db [262]	106 Sg [266]	107 Bh [264]	108 Hs [269]	109 Mt [268]	110 Uun [271]	111 Uuu [272]	112 Uub [277]	114 Uuq [289]					

Figure 11: Periodic table showing elements measurable by the Innov-X® X-Ray Fluorescence Spectrometer.

The XRF spectrometer measures elemental abundances by subjecting the sample to X-ray photons. The high energy of the photons displaces inner orbital electrons in the respective elements. The vacancies in the lower orbitals cause outer orbital electrons to “fall” into lower orbits to satisfy the disturbed electron configuration. The substitution into lower orbitals causes a release of a secondary X-ray photon, which has an energy associated with a specific element. These relative and element specific energy emissions can then be used to determine bulk elemental composition.

3.2 INDUSTRIAL CT SCANNING

Detailed scans of a section of interest (please refer to Section 4.3) were performed by the North-Star Imaging Inc. M-5000® Industrial Computed Tomography System shown in Figure 12 (Industrial CT) at NETL. The system was used to obtain higher resolution scans with a resolution of $(42.4 \mu\text{m})^3$ and capture the details of certain features clearly.

The scans were performed at a voltage of 185 kV and a current of 200 μA , which provided the best balance of resolution and energy to penetrate the samples. The samples were rotated 360° and 1,440 radiograph projections of the samples were obtained, averaging 10 individual radiographs at each step to create the reconstruction.

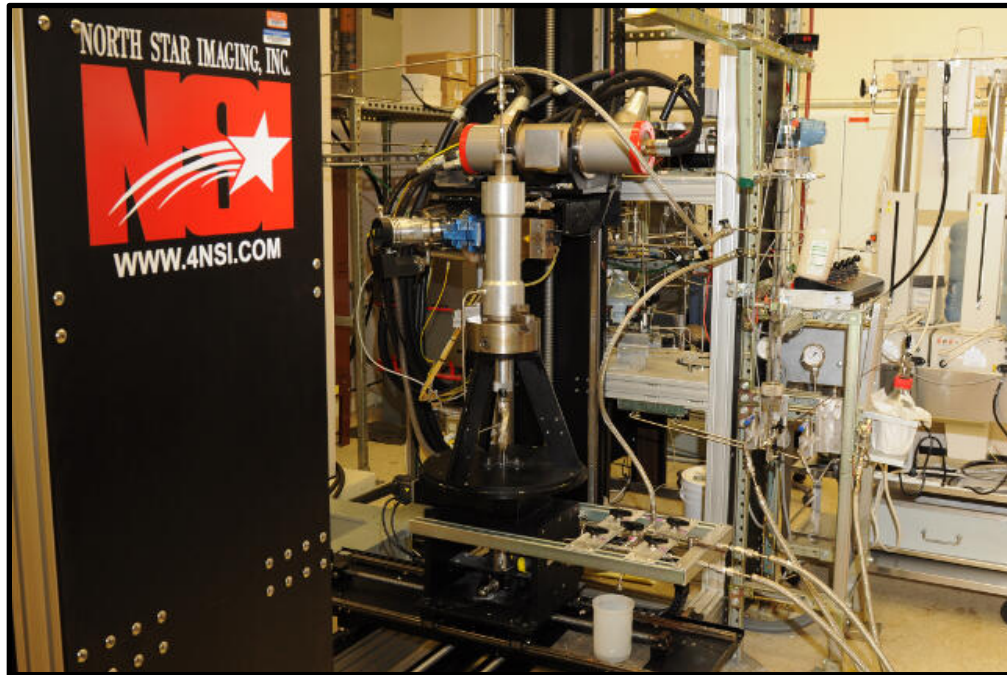


Figure 12: North Star Imaging Inc. M-5000® Industrial Computed Tomography Scanner at NETL used for core analysis.

3.3 MEDICAL CT SCANNING

Core scale CT scanning was done with a Toshiba® Aquilion TSX-101A/R medical scanner (medical CT) as shown in Figure 13. The medical CT scanner generates images with a resolution in the millimeter range, with scans having voxel resolutions of 0.43 x 0.43 mm in the XY plane and 0.50 mm along the core axis. The scans were conducted at a voltage of 135 kV and at a current of 200 mA. Subsequent processing and combining of stacks was performed to create three-dimensional (3D) volumetric representations of the cores and a two-dimensional (2D) cross-section through the middle of the core samples using ImageJ (Rasband, 2018). The variation in grayscale values observed in the CT images indicates changes in the CT number obtained from the CT scans, which is directly proportional to changes in the attenuation and density of the scanned rock. Darker regions are less dense. As can be seen in Figures 14–18, filled fractures, open fractures, and changes in bedding structure can all be resolved via careful examination of the CT images. While the medical CT scanner was not used for detailed characterization in this study, it allowed for non-destructive bulk characterization of the core, and thus complemented the MSCL data on the resultant logs.



Figure 13: Medical CT at the NETL used for core analysis.

3.4 DATA COMPILATION

Strater® by Golden Software® was used to compile the MSCL and medical CT data into a series of geophysical logs. The data used to generate these logs can be accessed from NETL's [EDX](https://edx.netl.doe.gov/dataset/roger-well) online system using the following link: <https://edx.netl.doe.gov/dataset/roger-well>.

4. RESULTS

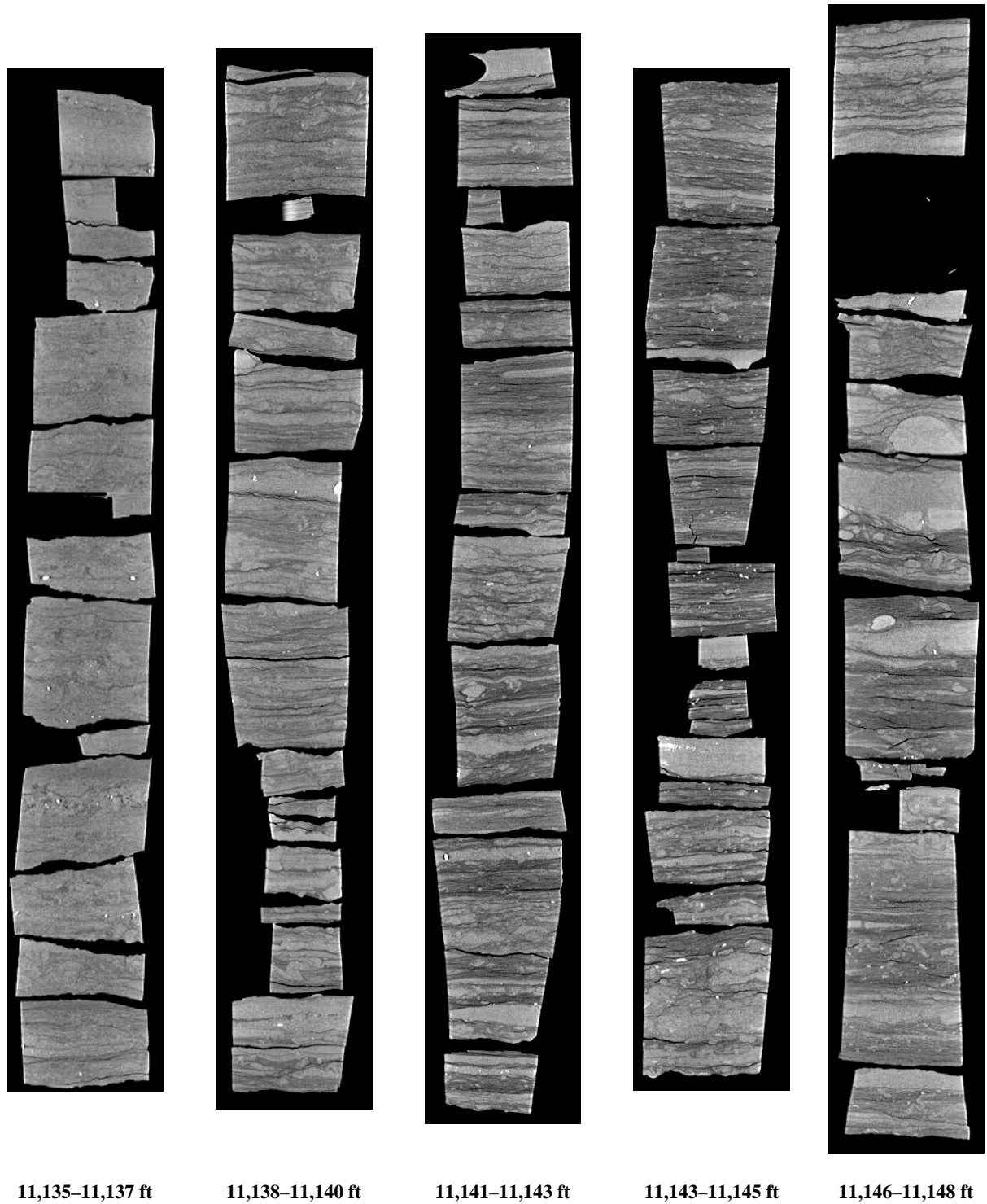
Processed 2D slices of the medical CT scans through the cores are shown first, followed by the XRF and magnetic susceptibility measurements of the core from the MSCL. The core from the Smith #1 well was scanned with a Toshiba Aquilion TSX-101A/R medical CT scanner at a sub-millimeter core-scale resolution (430 μm by 430 μm by 500 μm).

4.1 MEDICAL CT SCANS

As was discussed previously, the variation in grayscale values observed in the medical CT images indicates changes in the CT number obtained, which is directly proportional to changes in the attenuation and density of the scanned rock (i.e. darker regions are less dense).

Core was scanned in 2 ft or smaller sections. Highly-fractured regions with a true depth in excess of 2 ft were often scanned. Detailed information in log books and photographs of cores were used to merge multiple scans of cores when this occurred. In the following images, the overall depth for each scanned sub-section of core is listed and many interesting features can readily be seen, including pyrite nodules, defined fracture planes and fine scale layering.

4.2 SMITH #1



11,135–11,137 ft

11,138–11,140 ft

11,141–11,143 ft

11,143–11,145 ft

11,146–11,148 ft

Figure 14: 2D isolated planes through the vertical center of the medical CT scans of the Smith #1 core from 11,135 to 11,148 ft.

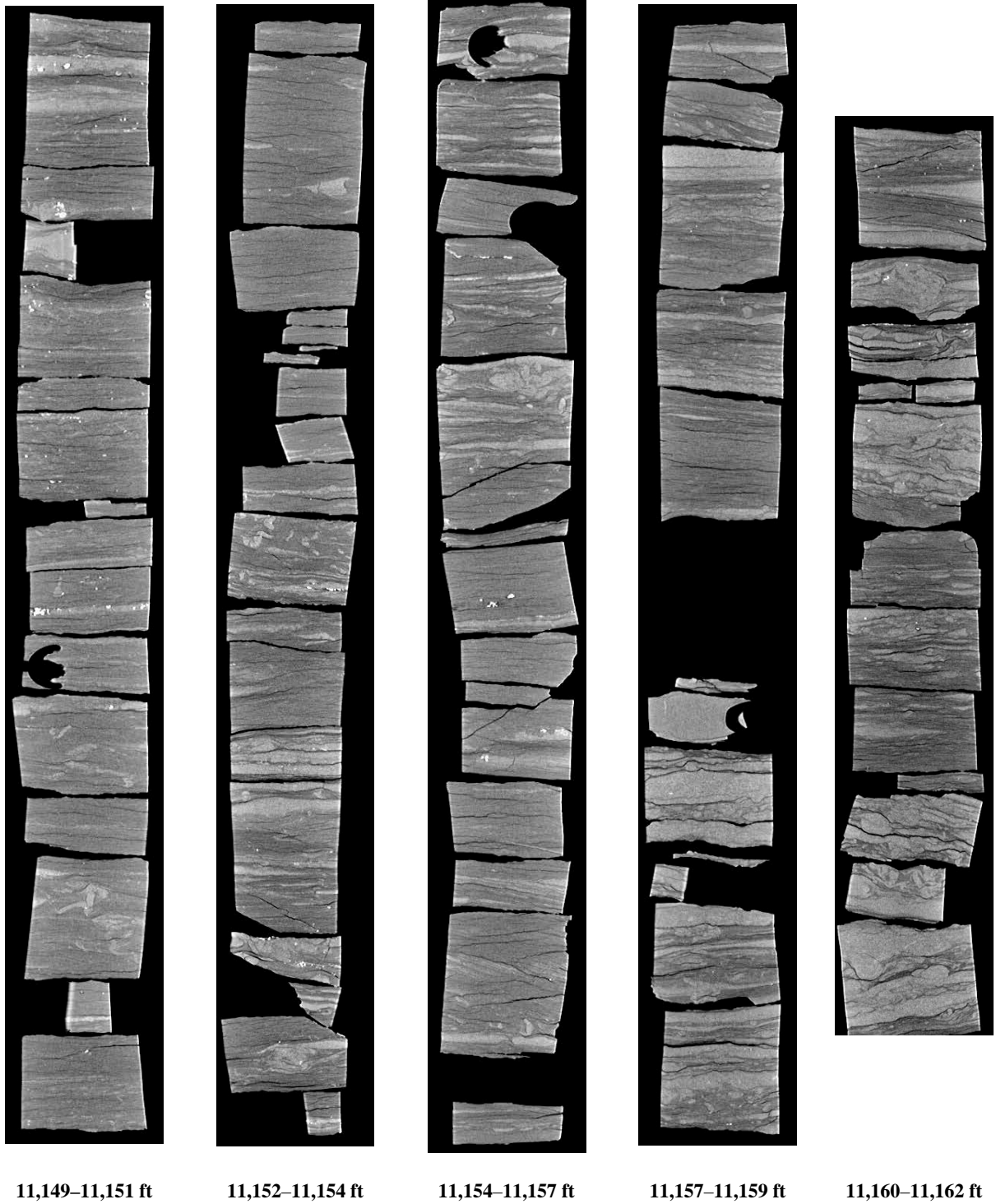
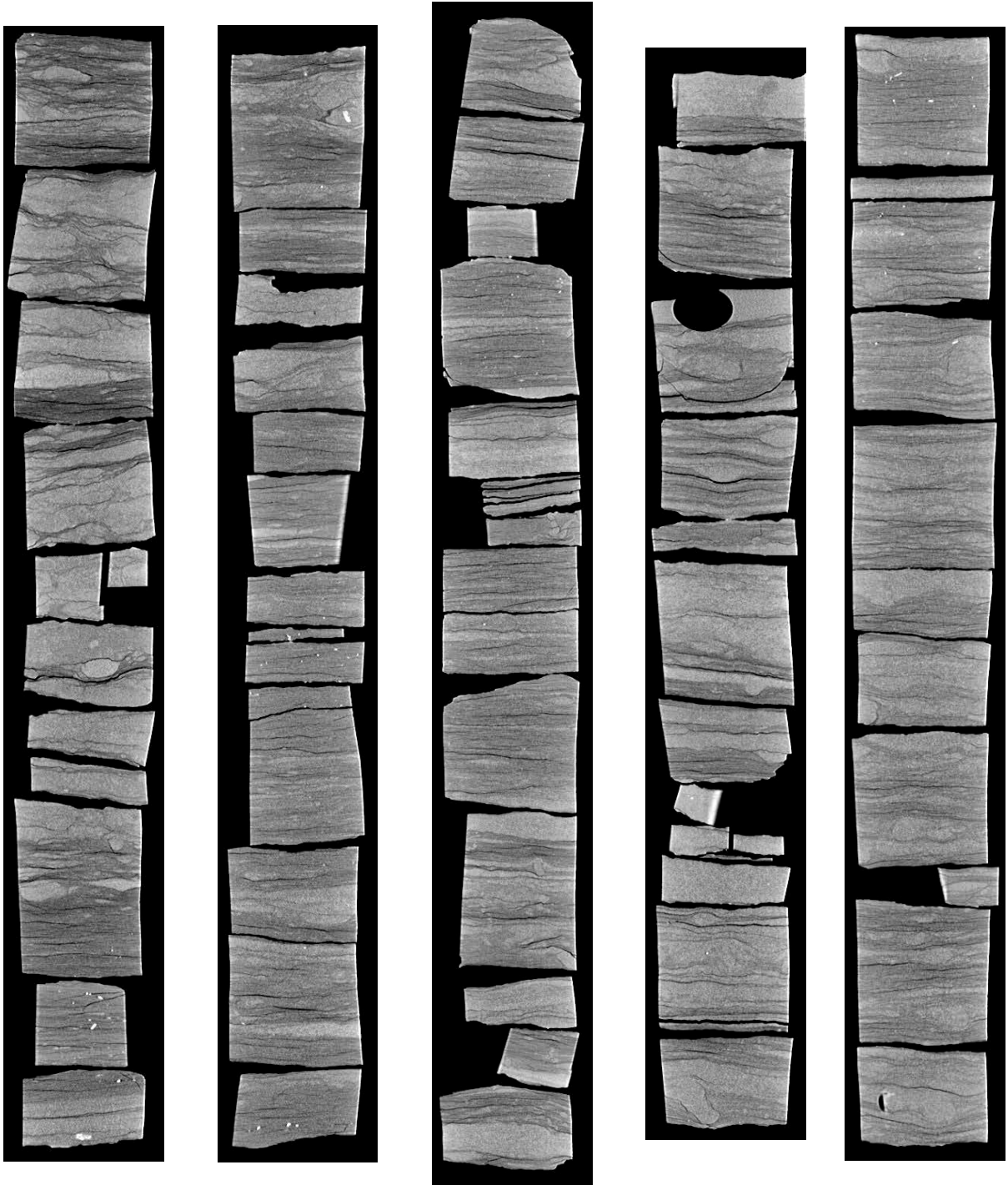


Figure 15: 2D isolated planes through the vertical center of the medical CT scans of the Smith #1 core from 11,149 to 11,162 ft.



11,162–11,165 ft

11,166–11,168 ft

11,168–11,171 ft

11,171–11,174 ft

11,174–11,177 ft

Figure 16: 2D isolated planes through the vertical center of the medical CT scans of the Smith #1 core from 11,162 to 11,177 ft.

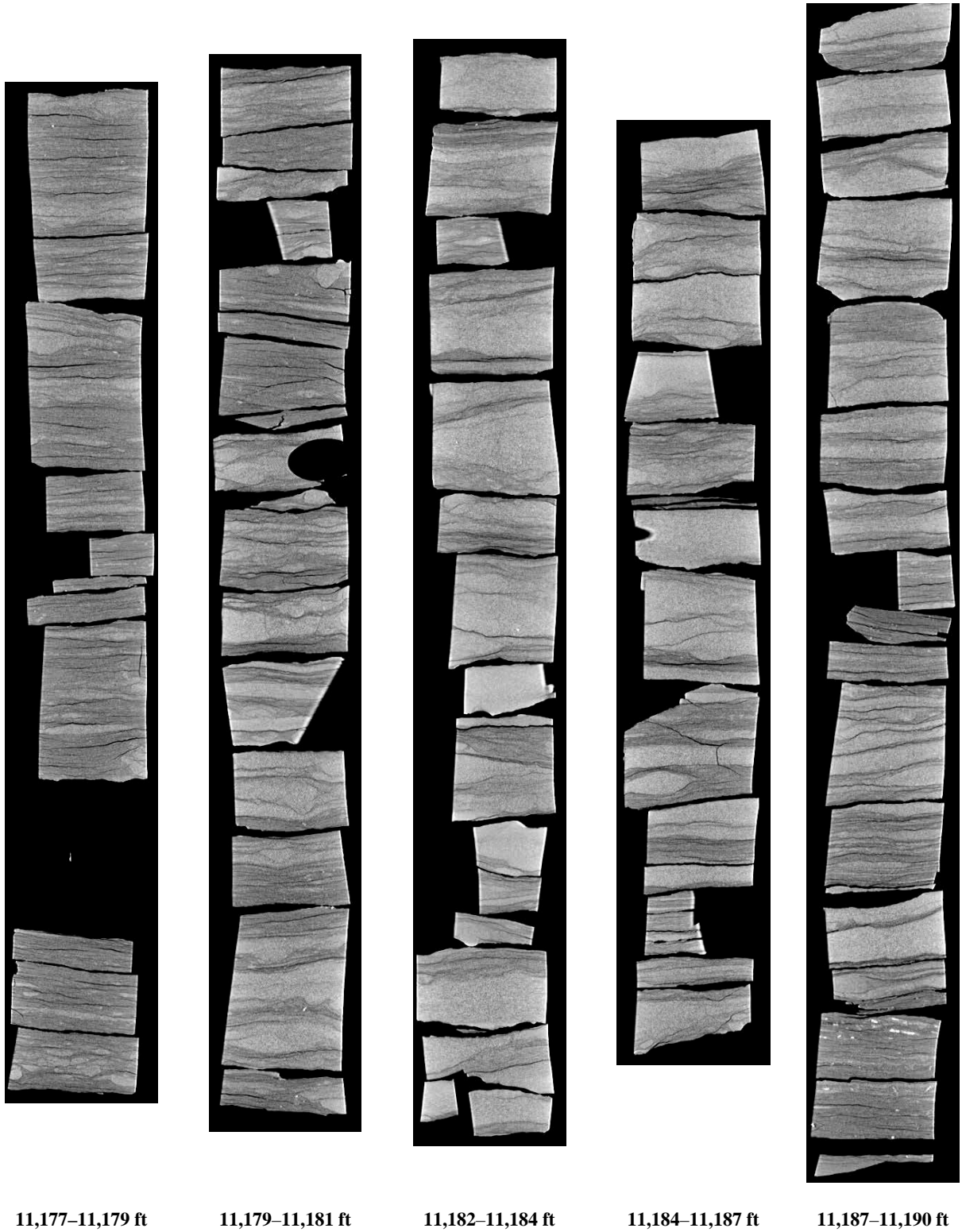


Figure 17: 2D isolated planes through the vertical center of the medical CT scans of the Smith #1 core from 11,177 to 11,190 ft.

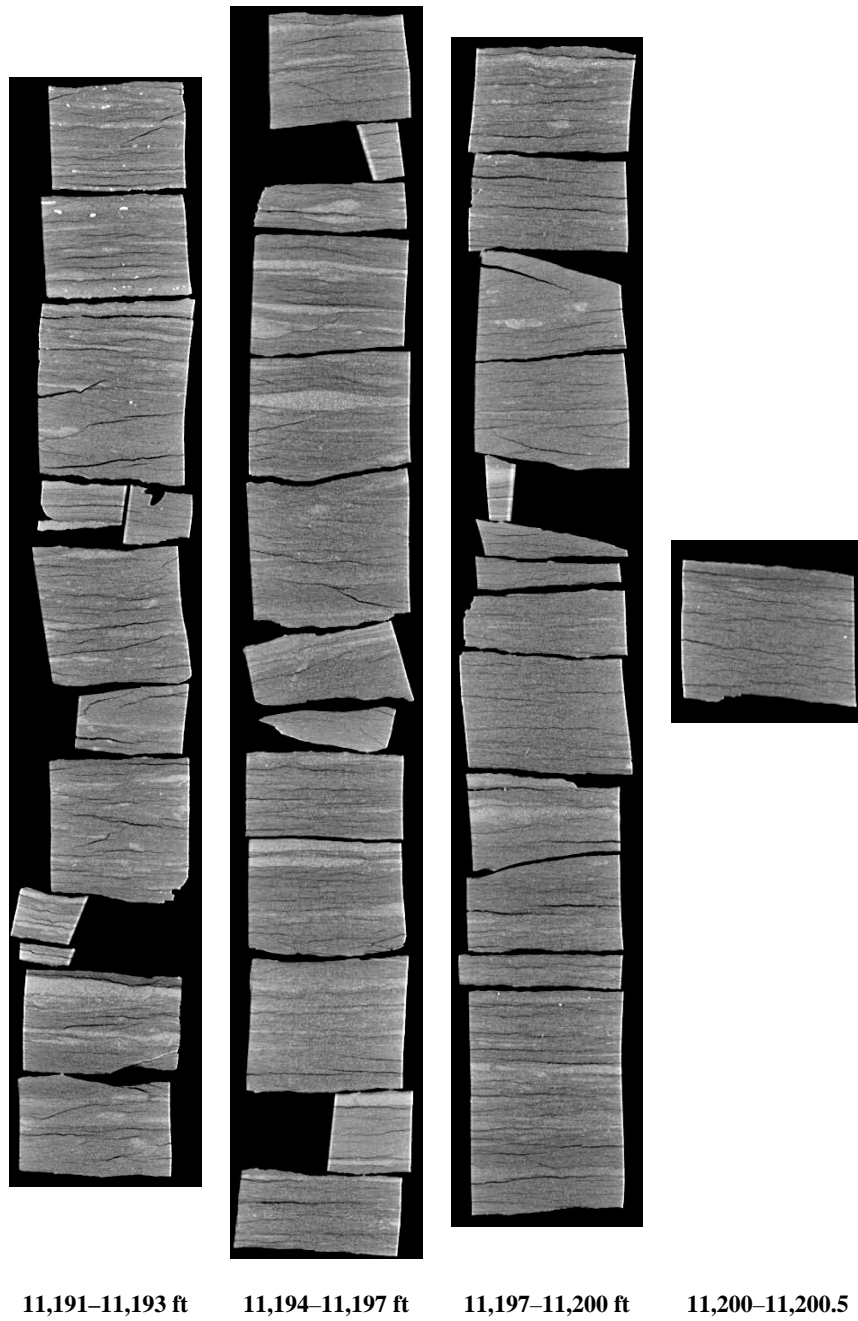


Figure 18: 2D isolated planes through the vertical center of the medical CT scans of the Smith #1 core from 11,191 to 11,200.5 ft.

4.3 INDUSTRIAL CT SCANS

The industrial CT scans were conducted at a resolution of $(42.4 \mu\text{m})^3$. The grayscale values in the following images were used to isolate and visually differentiate objects of interest in the scans, such as fractures and fine-grained regions, using the interactive learning and segmentation toolkit ilastik (Sommer et al., 2011). The features documented in these images provide a detailed analysis of the cores via industrial scanning.

The premise of isolating features is to first segment out the feature based on its unique grayscale value. Once this isolation has occurred, the next steps are to differentiate multiple isolated features and then combine them into one coherent visual representation. The following images show these feature isolations to enhance the ability of the reader to discern differences observed in the Smith #1 core. Only portions of the core were scanned and analyzed as part of this report because of the time involved in scanning with this system (over 2 hours per scan). Raw CT images are available for additional analysis on <https://edx.netl.doe.gov/dataset/roger-well>.

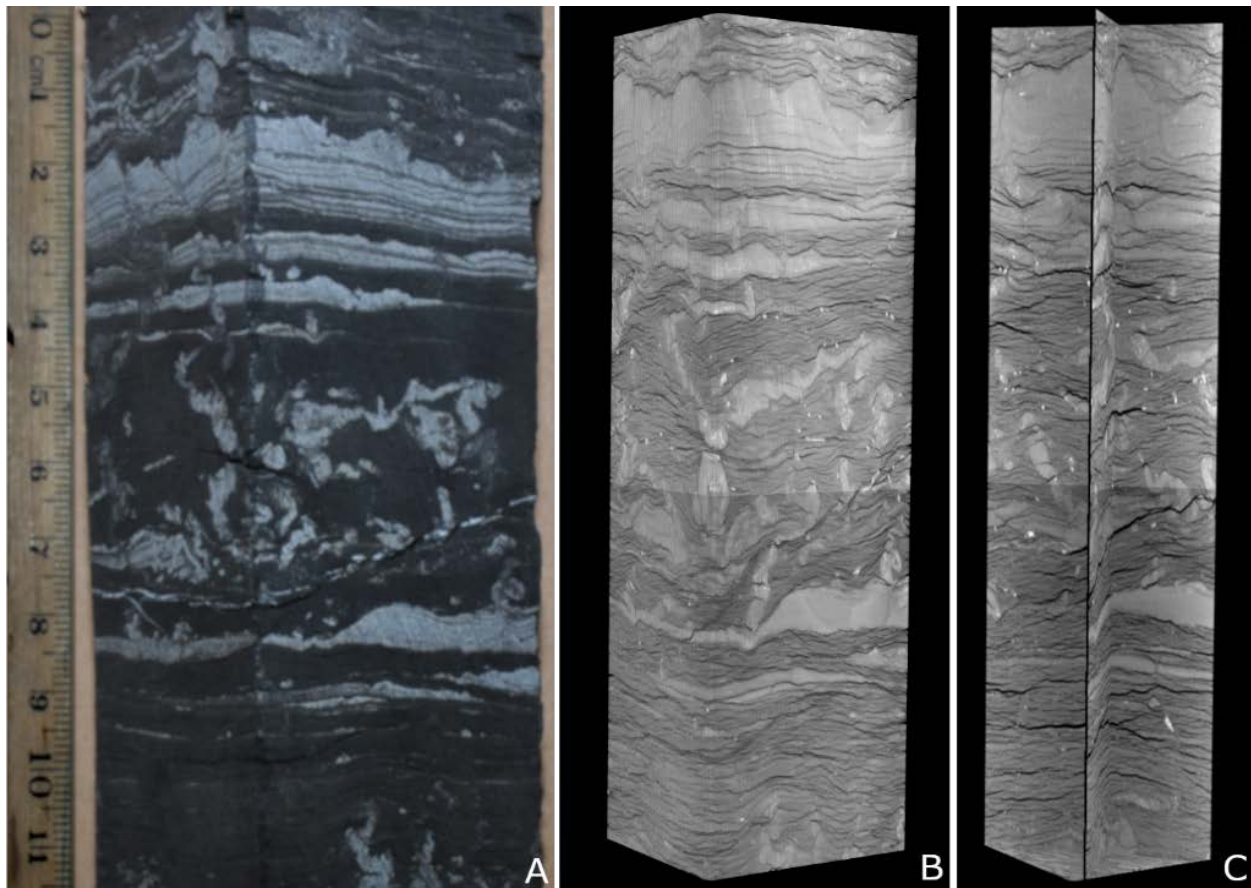


Figure 19: Visualization of features from the Smith #1 core at depth 11,147.5–11,147.9 ft. The images represent: A) Core photograph with scale in cm, B) 3D volumetric CT scan, C) Orthographic planes through the CT volume.

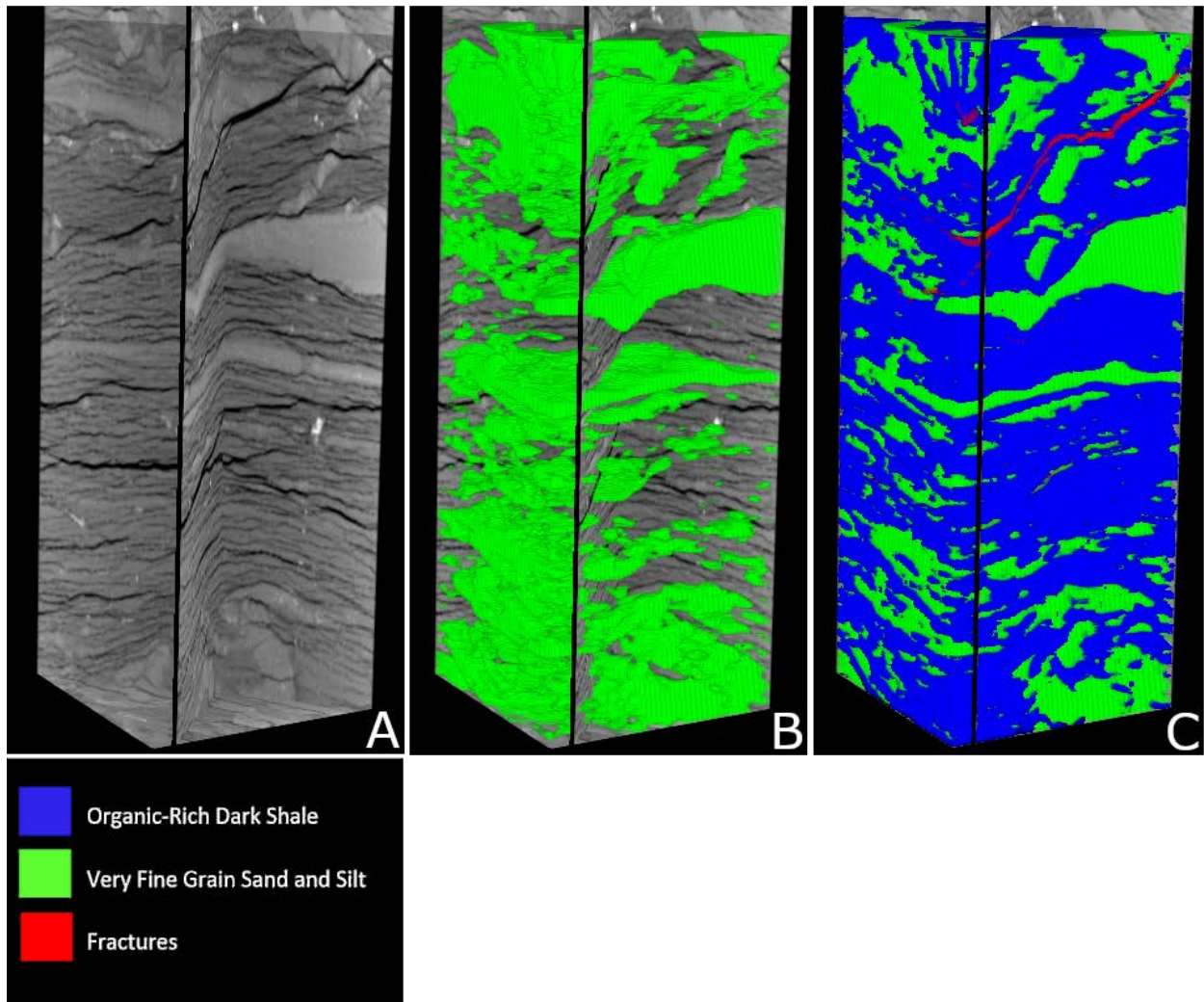


Figure 20: Visualization of features from the Smith #1 core at depth 11,147.7–11,147.9 ft. The images represent: A) orthographic planes through the CT volume, B) 3D volume of sand and silt in orthographic planes showing soft sediment deformation and filled burrows, and C) complete 3D volume with features distinguished by the colors from the legend.

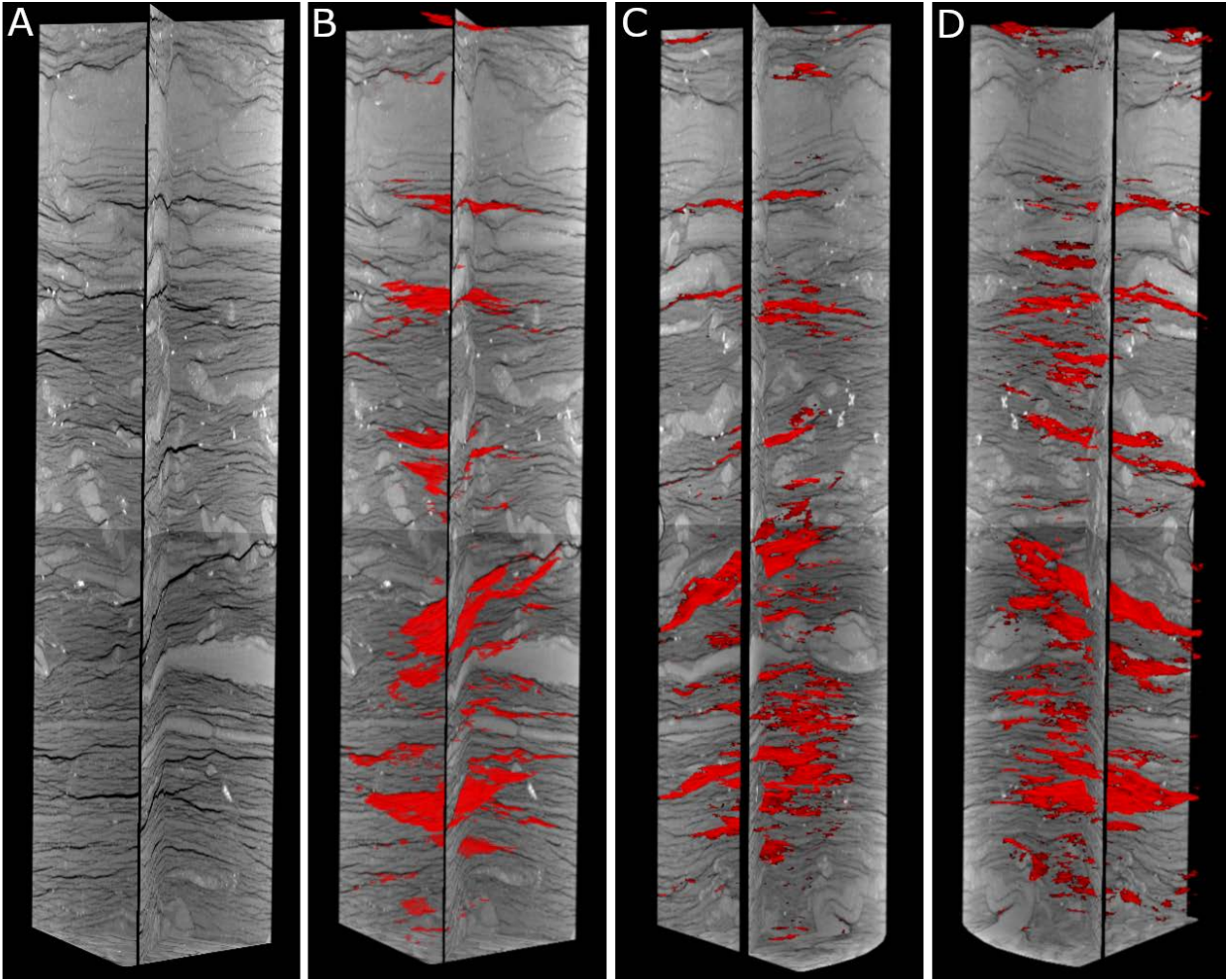


Figure 21: Representation of open fractures in the Smith #1 core at depth 11,147.5–11,147.9 ft. The images display: A) orthographic planes through the CT volume, B–C) 3D volume of fractures in orthographic planes shown at respective 0°, 120°, and 240° rotations.

4.4 ADDITIONAL CT DATA

Additional CT data can be accessed from NETL's EDX online system using the following link: <https://edx.netl.doe.gov/dataset/roger-well>. The original CT data is available as 16-bit tif stacks suitable for reading with ImageJ (Rasband, 2018) or other image analysis software. In addition, videos showing the variation along the length of the cross-section images shown in the previous section are available for download and viewing. A single image from these videos is shown in Figure 22, where the distribution of high density minerals in a cross section of the core around a depth of 11,161 ft is shown. Here, the red line through the diameter of the core shows the location of the XY-plane displayed above. The videos on <https://edx.netl.doe.gov/dataset/roger-well> show this XY variation along the entire length of the core.

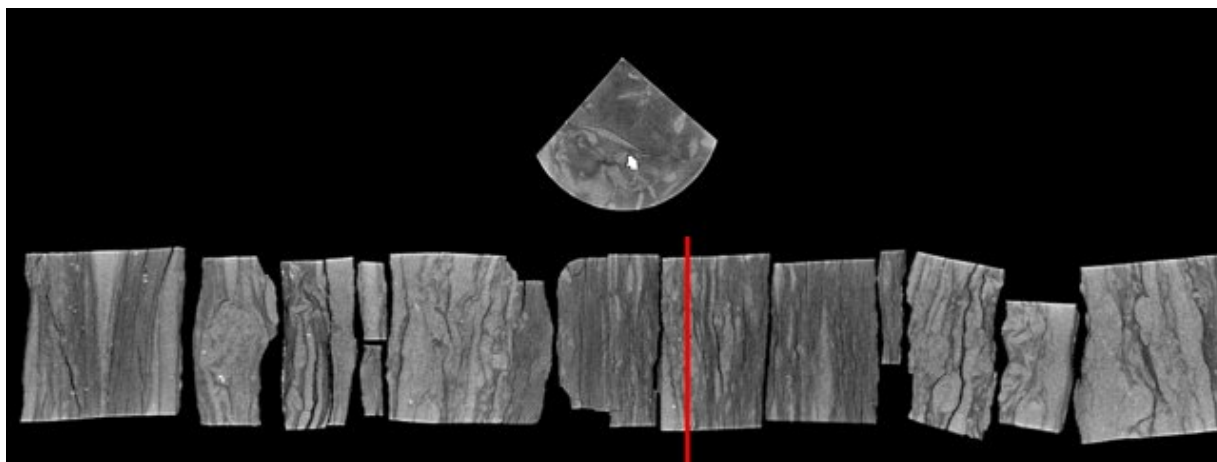


Figure 22: Single image from a video file available on EDX showing variation of the Smith #1 core from 11,160 to 11,162 ft. The image above shows the variation in composition within the matrix perpendicular to the core length. Note the bright (high density) nodule in the cross plane of the image.

4.5 DUAL ENERGY CT SCANNING

Dual energy CT scanning uses two sets of images, produced at different X-ray energies, to approximate the density (ρ_B) and the effective atomic number (Z_{eff}) (Siddiqui and Khamees, 2004; Johnson, 2012). The technique relies on the use of several standards of known ρ_B and Z_{eff} to be scanned at the same energies as the specimen. These scans are performed at lower energies (<100 KeV) and higher energies (>100 KeV) to induce two types of photon interactions with the object (Figure 23). The lower energy scans induce photoelectric absorption, which occurs when the energy of the photon is completely absorbed by the object mass and causes ejection of an outer orbital electron (Figure 23a). The high energy scans induce Compton scattering, which causes a secondary emission of a lower energy photon due to incomplete absorption of the photon energy in addition to an electron ejection (Figure 23b).

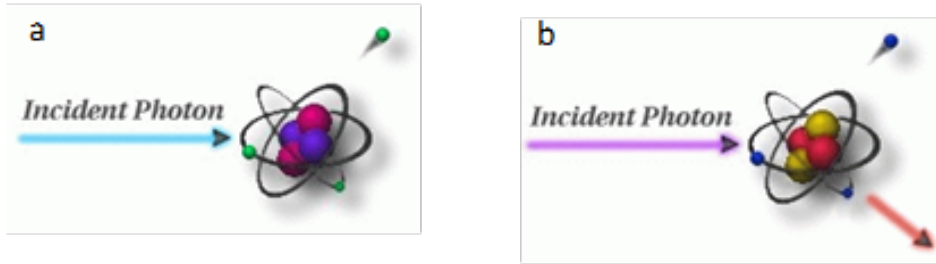


Figure 23: Photon interactions at varying energies: a) photoelectric absorption, b) Compton scattering. Modified from NDT Resource Center (2018).

Medical grade CT scanners are typically calibrated to known standards, with the output being translated in CT numbers (CTN) or Hounsfield Units (HU). Convention for HU defines air as -1000 and water as 0. A linear transform of recorded HU values is performed to convert them into CTN. This study used CTN as it is the native export format for the instrument, but it is possible to use HU. Dual energy CT requires at least 3 calibration points and it is prudent to utilize standards that approximate the object or material of interest. Pure samples of aluminum, graphite, and sodium chloride were used as the calibration standards as they most closely approximate the rocks and minerals of interest (Table 2). Most materials denser than water or with higher atomic masses have a non-linear response to differing CT energies (Table 2).

Table 2: Dual energy calibration standards

Material	ρ_B (g/cm ³)	Z_{eff}
Air	-0.001	7.22
Water	1	7.52
Graphite	2.3	6
Sodium Chloride	2.16	15.33
Aluminum	2.7	13

Table 3: Dual energy calibration standards

Material	HU		CTN	
	80 KeV	135 KeV	80 KeV	135 KeV
Air	-993	-994	31,775	31,774
Water	-3.56	-2.09	32,764	32,766
Graphite	381	437	33,149	33,205
Sodium Chloride	1,846	1,237	34,614	34,005
Aluminum	2,683	2,025	35,451	34,793

Dual energy CT utilizes these differences to calibrate to the X-ray spectra. Two equations with 3 unknowns each are utilized to find ρ_B and Z_{eff} (Siddiqui and Khamees, 2004):

$$\rho_B = mCTN_{\text{low}} + pCTN_{\text{high}} + q$$

$$Z_{\text{eff}} = \sqrt[3.6]{\frac{(rCTN_{\text{low}} + sCTN_{\text{high}} + t)}{(0.9342 * \rho_B + 0.1759)}}$$

Where [m, p, and q] and [r, s, and t] are unknown coefficients that can be solved by setting up a system of equations with four 3 x 3 determinants. The CTN is obtained from the CT scans for each of the homogenous calibration standards.

In this study the high and low energy image stacks were loaded into Python as arrays. A 3-D Gaussian blur filter with a sigma of 2 was used to reduce noise in the images. The `scipy.solve` module of Python was then employed to solve for the coefficients based on the calibration CTN values. The ρ_B and Z_{eff} were both solved for each pixel in the 3D volume and saved as two new separate image stacks.

ImageJ (Rasband, 2018) was used to reslice the image stacks to produce 2D representative cross-sections of the entire core-length. A 6-shade look up table was used to apply a gradational color scale to the image with the total range of values limited to densities from 2 to 4.5 g/cm³; this eliminated much of the noise in the air portion of the scans and at the edges of the sample. The average density along the length of the cores was calculated by excluding all densities below 2 g/cm³. This study assumed that the cores were free of water and liquids as they were air dried and that the cores do not contain an appreciable quantity of elements with densities lower than 2.0 g/cm³.

4.6 COMPILED CORE LOG

The compiled core logs were scaled to fit on single pages for rapid review of the combined data from the medical CT scans and MSCL readings. Due to the total length of the core, the data is presented along two intervals, from 11,135–11,168 ft and 11,168–11,200.5 ft to enable visualization. Two sets of logs are presented for each section, the first set with data from the CT scans, magnetic susceptibility and raw XRF values and the second set with calculated ratios from the XRF scans, P-wave velocity, CT derived dual energy density, and notable features from the core listed.

Data from the MSCL that was obtained with P-wave velocity less than 330 m/s has been removed from these logs. This low P-wave velocity is less than the anticipated velocity through air, indicating a highly fractured zone and unreliable readings. The locations of these fractured zones were confirmed through visual examination and with the medical CT scanned images.

The elemental results from the XRF were limited to Ca, Si and the remaining top ten elements (S, Al, Fe, K, Mg, Ti, P, Zn, Mn, and V). Of the remaining top ten elements, S was the most abundant with a maximum occurrence of 99,403 ± 359 ppm at one location in the core, and V was the least abundant element with a maximum occurrence of 577 ± 48 ppm at one location in

the core. All other elements measured (Figure 11), but not listed, were observed to have maximum occurrences of less than 350 ppm.

These combined analyses enable determination of mineral phases present (such as pyrite) from magnetic susceptibility and geochemical compositions. More specifically, trends in elemental ratios can provide insight into mineral composition, oxidation state and depositional setting. Examples include: Ca/Si, which provides information on relative abundance of calcium carbonates versus silicates; Ca/Al, which gives approximate amounts of calcium carbonate versus clays and feldspar; and K/Al, which provides information on the abundance of illite and micas versus other clays. Magnetic susceptibility can test for Fe sulfides (reducing) or oxidized Fe and sulfate. Pyrite (reduced) should have low magnetic susceptibility. Fe oxide or hydroxide should have high magnetic susceptibility. Natural gamma is a proxy for organic carbon as well. These broad trends can quickly give information on large suites of core and direct more focused research. The CT derived dual energy density calculations were cropped at 2.2 g/cm³.

These logs are presented in the following images, Figures 24–27.

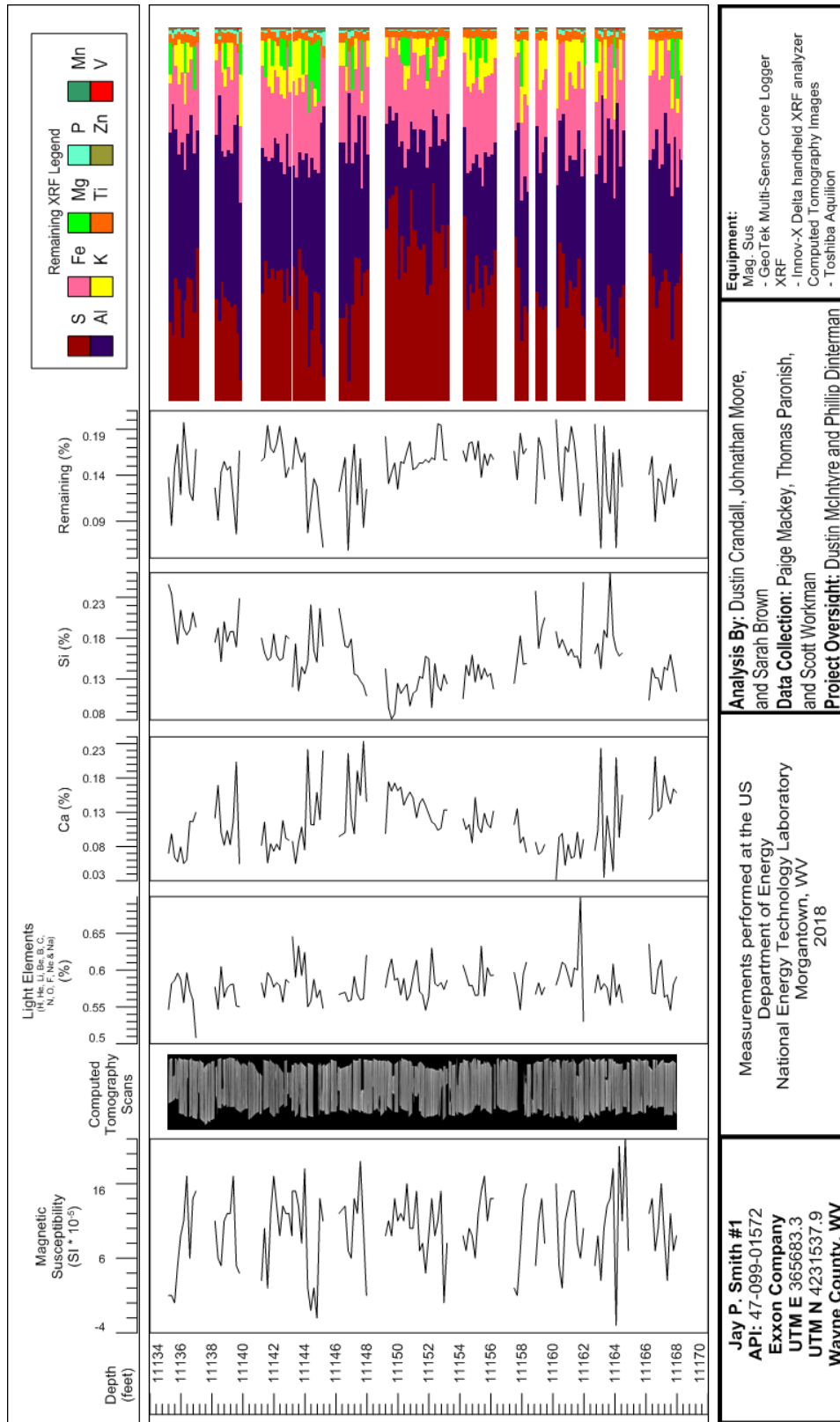


Figure 24: Compiled core log for Smith #1 well, from 11,135 to 11,168 ft.

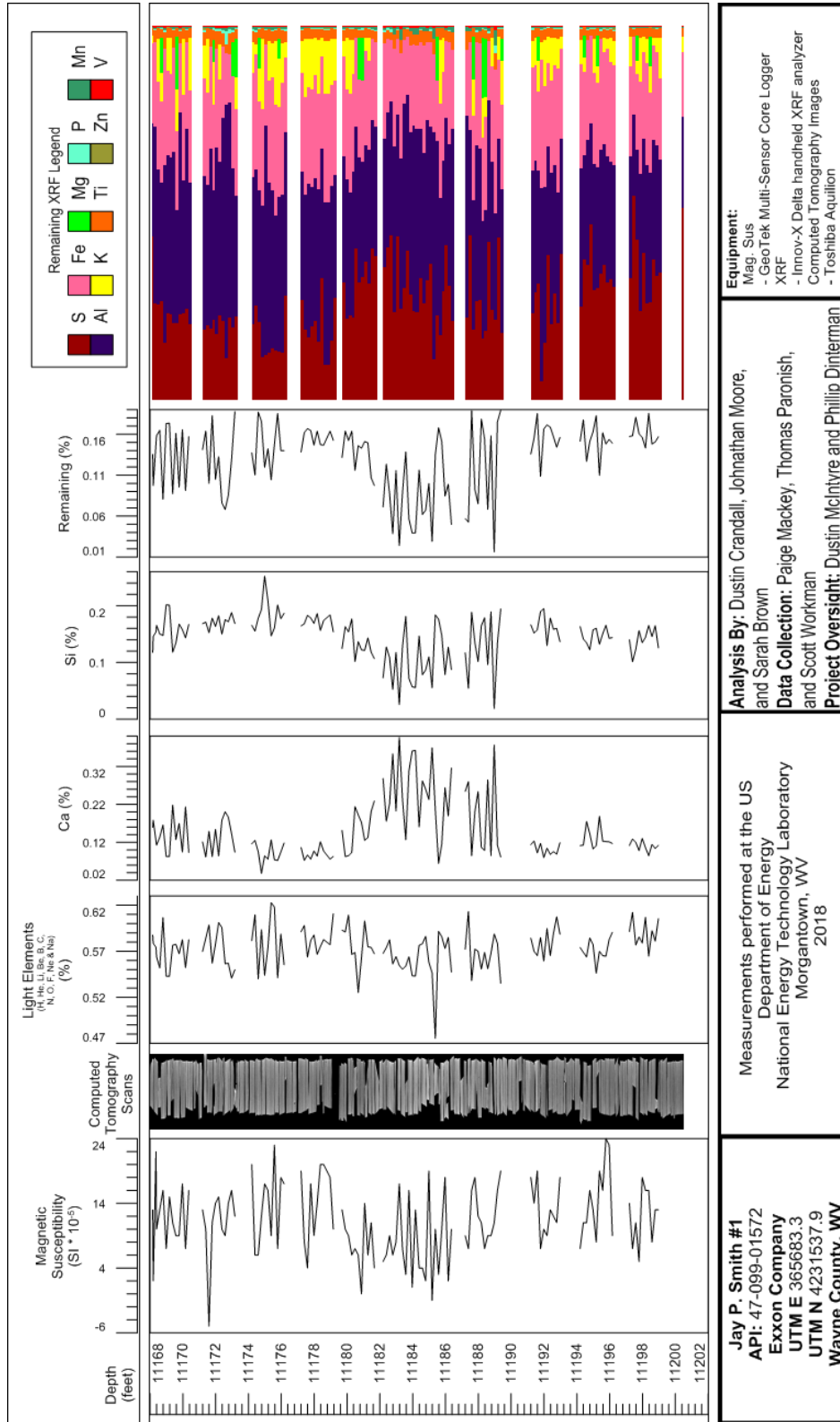


Figure 25: Compiled core log for Smith #1 well, from 11,168 to 11,200 ft.

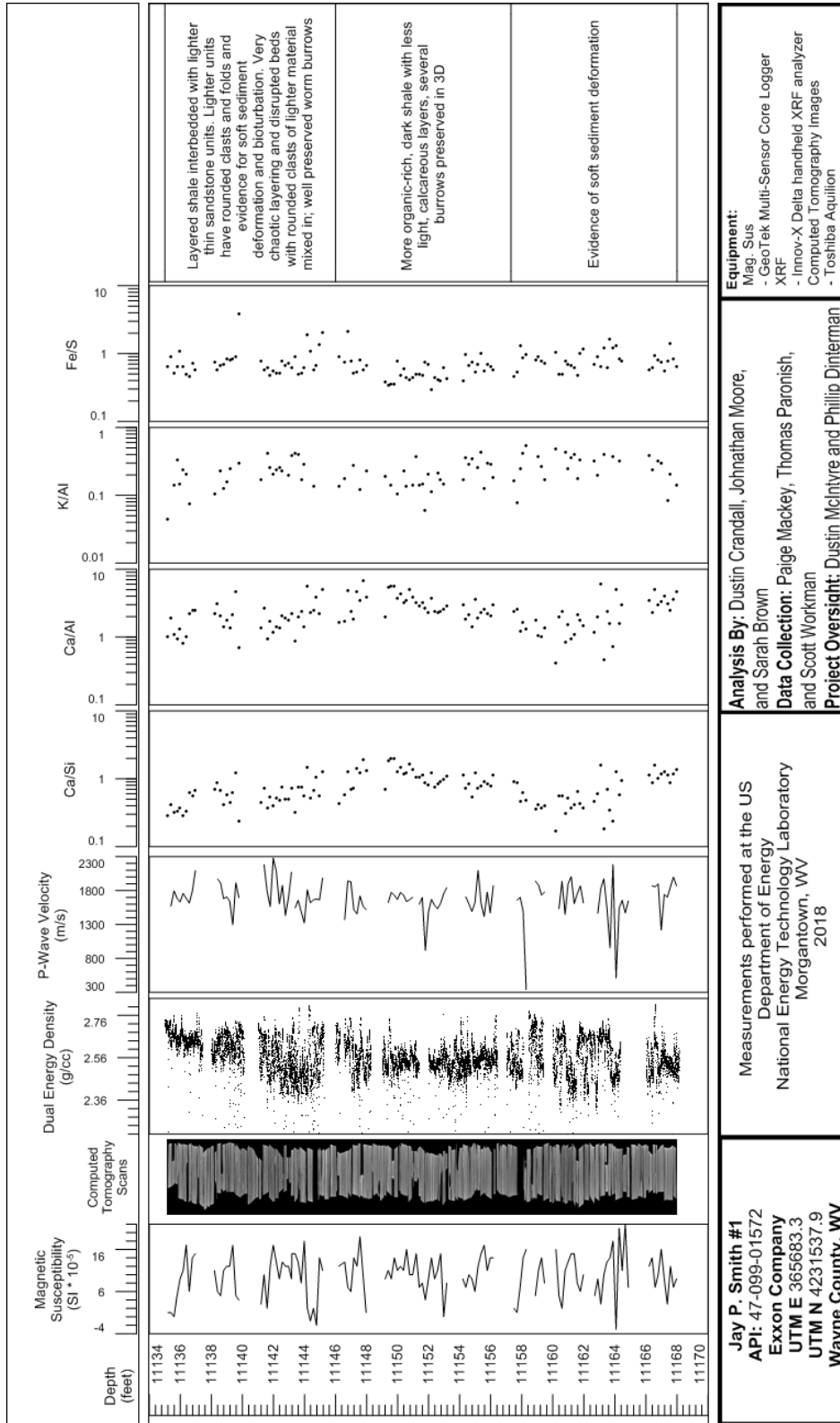


Figure 26: Compiled core log with elemental ratios for Smith #1 well, from 11,135 to 11,168 ft.

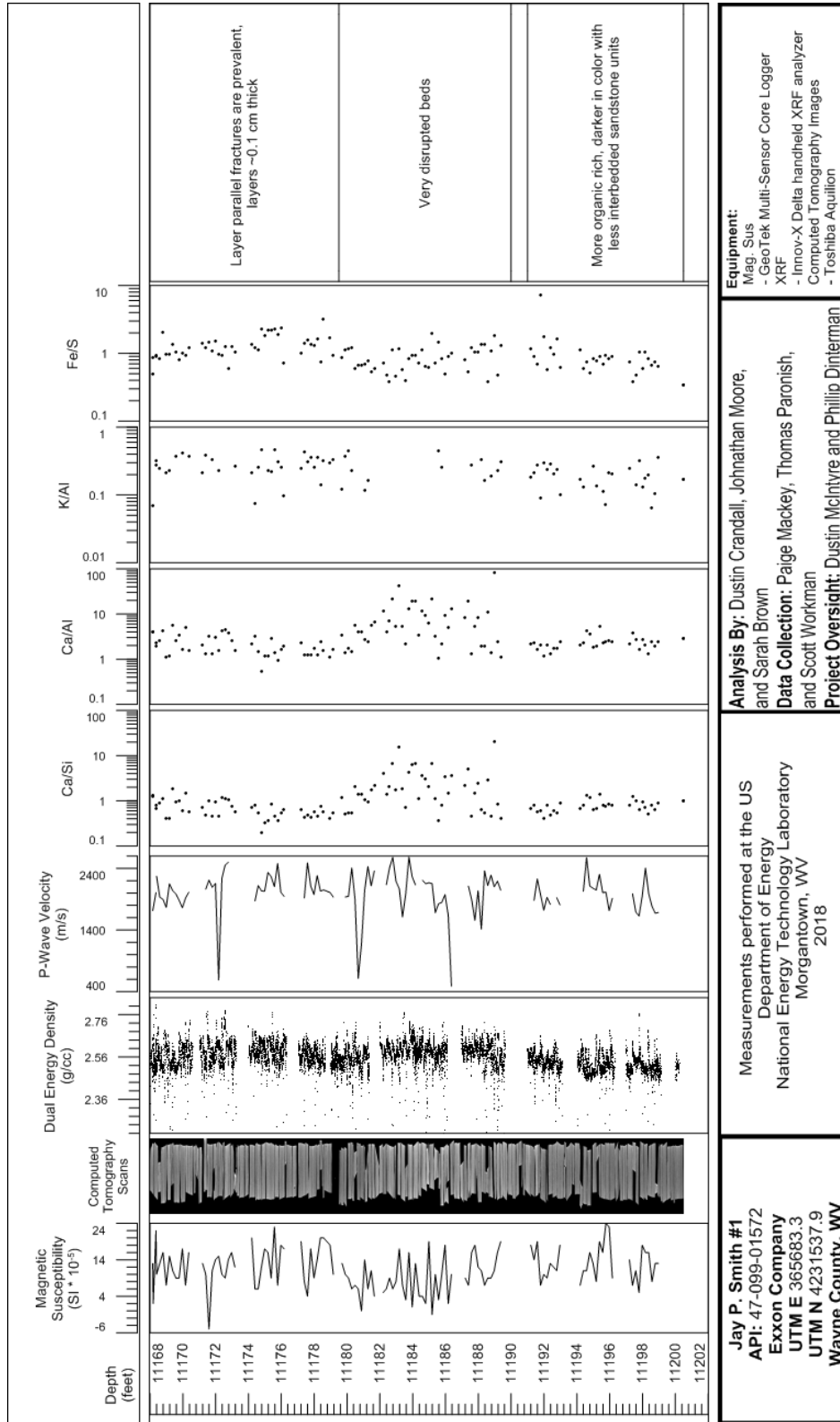


Figure 27: Compiled core log with elemental ratios for Smith #1 well, from 11,168 to 11,200 ft.

5. DISCUSSION

The measurements of the magnetic susceptibility, P-wave velocity, XRF, and CT analysis provide a unique look into of the internal structure of the core and macroscopic changes in lithology. These techniques:

- Are non-destructive
- When performed in parallel give insight into the core beyond what one individual technique can provide
- Can be used to identify zones of interest for detailed analysis, experimentation, and quantification
- Provide a detailed digital record of the core, before any destructive testing or further degradation, that is accessible and can be referenced for future studies

This page intentionally left blank.

6. REFERENCES

- Crandall, D.; Moore, J.; Brown, S.; Martin, K.; Mackey, P.; Paronish, T.; Carr, T.; Bowers, C. *Computed Tomography Scanning and Geophysical Measurements of Core from the Coldstream 1MH Well*; NETL-TRS-5-2018; NETL Technical Report Series; U.S. Department of Energy, National Energy Technology Laboratory: Morgantown, WV, 2018a; p 48.
- Crandall, D.; Moore, J.; Rodriguez, R.; Gill, M.; Soeder, D.; McIntyre, D.; Brown, S. *Characterization of Martinsburg Formation using Computed Tomography and Geophysical Logging Techniques*; NETL-TRS-4-2017; NETL Technical Report Series; U.S. Department of Energy, National Energy Technology Laboratory: Morgantown, WV, 2017; p 68.
- Crandall, D.; Paronish, T.; Brown, S.; Martin, K.; Moore, J.; Carr, T.R.; Panetta, B. *CT Scanning and Geophysical Measurements of the Marcellus Formation from the Tippens 6HS Well*; NETL-TRS-3-2018; NETL Technical Report Series; U.S. Department of Energy, National Energy Technology Laboratory: Morgantown, WV, 2018b; p 32.
- Geotek Ltd. Geotek Multi-Sensor Core Logger Flyer, Daventry, UK, 2009.
<http://www.geotek.co.uk/sites/default/files/MSCLOverview.pdf>
- Geotek Ltd. Multi-Sensor Core Logger Manual; Version 05-10; Published by Geotek, 3 Faraday Close, Daventry, Northamptonshire NN11 8RD, 2010. info@geotek.co.uk,
www.geotek.co.uk.
- Harris, D. C.; Drahozal, J.A.; Hickman, J.G.; Nuttall, B.C.; Baranoski, M.T.; Avary, K.L. Rome Trough Consortium Final Report and Data Distribution: Kentucky Geological Survey Report 5875, OF_04-0006_12; 2004.
- Hickman, J.; Harris, D.; Eble, C. *Cambrian Rogersville Shale in the Rome Trough, Kentucky and West Virginia: A Potential Unconventional Oil and Gas Reservoir in the Appalachian Basin*; Kentucky Geological Survey, AAPG June 2015, (accessed April 2018).
- Johnson, T. R. C. Dual-Energy CT: General Principles. *American Journal of Roentgenology* **2012**, 199(5_supplement), S3–S8. DOI: 10.2214/AJR.12.9116.
- Rasband, W. S. ImageJ. U.S. National Institutes of Health: Bethesda, MD, 1997–2016,
<http://imagej.nih.gov/ij/> (accessed 2018).
- Ryder, R. T.; Harris, D. C.; Gerome, P.; Hainsworth, T. J.; Burruss, R. C.; Lillis, P. G.; Jarvie, D. M.; Pawlewicz, M. J. Evidence for Cambrian petroleum source rocks in the Rome trough of West Virginia and Kentucky, Appalachian basin, Chap. G.8 of *Coal and Petroleum Resources in the Appalachian basin; Distribution, geologic framework, and geochemical character*; Ruppert, L. F., Ryder, R. T., Eds.; U.S. Geological Survey Professional Paper 1708, 2014; p 36; Chapter G.8 supersedes USGS Open-File Report 2005–1443.
<http://dx.doi.org/10.3133/pp1708G.8>
- Siddiqui, S.; Khamees, A. A. Dual-Energy CT-Scanning Applications in Rock Characterization. *Society of Petroleum Engineers* 2004. DOI:10.2118/90520-MS.

Sommer, C.; Strähle, C.; Köthe, U.; Hamprecht, F.A. ilastik: Interactive Learning and Segmentation Toolkit; Proceedings of Eighth IEEE International Symposium on Biomedical Imaging (ISBI), 2011; 230–233.

Sources of Attenuation. Nondestructive Testing Resource Center, www.nde-ed.org/EducationResources/CommunityCollege/Radiography/Physics/attenuation.htm (accessed 2018).



Sean Plasynski, Ph.D.
Director (Acting)
National Energy Technology Laboratory
U.S. Department of Energy

Jared Ciferno
Associate Director
Oil and Gas
Technology Development & Integration
Center
National Energy Technology Laboratory
U.S. Department of Energy

Elena Melchert
Director
Division of Upstream Oil and Gas
Research
U.S. Department of Energy

Bryan Morreale
Executive Director
Research and Innovation Center
National Energy Technology Laboratory
U.S. Department of Energy